Operando Differential Electrochemical Pressiometry for Probing Electrochemo-Mechanics in All-Solid-State Batteries

Seunggoo Jun, Young Jin Nam, Hiram Kwak, Kyu Tae Kim, Dae Yang Oh, and Yoon Seok Jung*

Owing to an absence or lack of soft (and/or liquid) components, electrochemo-mechanical effects are imperative for all-solid-state batteries (ASBs) based on inorganic solid electrolytes (SEs). As this aspect has been overlooked, relevant investigation has remained scarce. In this work, the development of a new operando differential electrochemical pressiometry (DEP) for ASBs is reported. The time- (or capacity-) derivative differential pressure signals (dP/dt or dP/dQ) reflecting corresponding differential volume changes of electrode active materials feature the specific state of charges (SOCs). This finding leads to a precise estimation of the SOCs of graphite (Gr) electrodes in $LiNi_{0.70}Co_{0.15}Mn_{0.15}O_2$ (NCM)/Gr all-solid-state full cells using sulfide SEs with varying capacity ratios of negative to positive electrodes (n/p ratios); this is corroborated by complementary analysis using a three-electrode electrochemical cell and ex situ X-ray diffraction measurements. Furthermore, electrochemo-mechanical behaviors of NCM/Gr full cells with Gr electrodes employing SEs excluding or including reductively unstable $Li_{10}GeP_2S_{12}$ are investigated. Notable volume changes caused by lithiation of $Li_{10}GeP_2S_{12}$ are detected. Importantly, significantly delayed SOC for Gr caused by a severe side reaction with $Li_{10}GeP_2S_{12}$ is disclosed by the operando DEP result.

1. Introduction

In lithium-ion battery (LIB) technologies, volume change in electrode active materials has been one of the prime factors influencing material-to-cell design.[1–6] Integrating silicon anodes to advanced LIBs requires multiple aspects of engineering including downsizing to the nanometer scale,[3,7–10] nanocompositing with buffering phases,[3,7,9,10] combining highly adhesive and/or elastic polymeric binders,[11–13] and the use of optimized electrolyte recipes.[1,14,15] This is owing to the large volumetric strain of Si ($\approx$400%, Si $\rightarrow$ $Li_{4.4}Si$), which

causes electrical contact loss and perpetual electrolyte decomposition reactions on newly exposed surfaces.[1,3,9,14,15] For high-Ni $Li[Ni,Co,Mn]O_2$ cathode cycled at over $\approx$4.3 V (vs Li/Li^+), volumetric strains of $>\approx$4% induce the disintegration of secondary particles, thus leading to performance degradation in long-term cycling.[16–18] Furthermore, the volume changing feature of electrode active materials in LIBs has been extended for use in actuation targeting of microelectromechanical systems.[19]

The current LIBs have faced serious challenges in terms of safety and high energy density, which largely originates from the use of flammable organic liquid electrolytes.[4,20–22] In this regard, solidification of electrolytes with inorganic solid electrolyte (SE) materials has garnered considerable interest.[21–30] To date, research activities on all-solid-state batteries (ASBs) have been focused on the development of SE materials in consideration of Li^+ transport and conductivity, chemical stability, electrochemical stability, and (electro)chemical compatibility with electrode active materials.[21,22,26,31–36] Specifically, studies on the dynamic evolution at the electrode-SE interface have put an emphasis on (electro)chemical aspects.[17,32,37,38]

It was not until very recently that attention has been paid to electrochemo-mechanical effects for ASBs.[6,37,39–41] The defective feature of 2D contacts between inorganic solid components in ASBs could be considerably amplified, even by small volumetric strains of electrode active materials; this is reflected in the common practice wherein all-solid-state test cells are operated under externally applied pressure.[17,22,42,43] Recent investigations have reported that the increase in external pressure on all-solid-state Li metal batteries results in significantly reduced interfacial resistances and increased critical currents against internal short circuits, which is rationalized by pressure-induced close contacts between SEs and Li metal.[44,45] Moreover, it is an important feature that SEs cannot access the disintegrated inner parts of the electrode active materials, in stark contrast to the case of conventional LIBs using liquid electrolytes. The aforementioned features are partly responsible

S. Jun, Dr. Y. J. Nam, H. Kwak, K. T. Kim, Dr. D. Y. Oh, Prof. Y. S. Jung
Department of Energy Engineering
Hanyang University
Seoul 04763, South Korea
E-mail: yoonsjung@hanyang.ac.kr

for below-par electrochemical performances of all-solid-state batteries despite the use of sufficiently high Li$^+$ conductivities of >10^{-3} S cm^{-1}.[17]

One major differentiating characteristic of ASBs from the viewpoint of performance is the absence or lack of soft (and/or liquid) components that can buffer volumetric strains and provide opportunities for advanced characterization.[6,17] Janek and coworkers showed that, while the effect of typically applied pressures (of up to hundreds of MPa) on potential is insignificant, the pressure changes upon charge and discharge, which reflect the corresponding volume changes of electrode active materials, could be measured.[6,40] In our recent report, by cross-sectional scanning electron microscopy (SEM) measurements, it was shown that LiNi$_{0.80}$Co$_{0.10}$Mn$_{0.10}$O$_2$ particles in all-solid-state cells were disintegrated and void spaces were created even after the initial cycle, which could be well-supported by the pressure measurement data.[17]

For commercial LIBs, the negative electrode is balanced with an excess capacity in the range of 10–20% with respect to the positive electrode, i.e., n/p ratios of 1.1–1.2, which have been optimized in order to minimize the risk of detrimental Li metal growth on the negative electrodes.[46] In some cases, a combination of two electrodes, each of which shows stable cycling performances in half cells, could result in fast degradation in full cells.[47] One possible failure mode is poorly balanced Coulombic efficiencies (CEs) between two electrodes, which leads to gradually increasing deviation in their SOCs.[46] As such, the estimation of SOCs is imperative for both LIBs and practical ASBs.

Here, we report the development of new operando differential electrochemical pressiometry (DEP) for ASBs. The pressure changes during charging and discharging were explicitly monitored in real time for LiNi$_{0.70}$Co$_{0.15}$Mn$_{0.15}$O$_2$ (NMC)/graphite (Gr) all-solid-state full cells employing sulfide SEs with varying n/p

ratios as a model system. Importantly, for the first time, the precise estimation of the state of charges (SOCs) of one electrode (Gr) was enabled by the analysis of the DEP profiles, which was corroborated by meticulous analysis using a three-electrode cell and ex situ X-ray diffraction (XRD) measurements. Furthermore, NCM/Gr full cells employing two different SEs in the Gr electrodes, that were both without and with reductively unstable Li$_{10}$GeP$_2$S$_{12}$ (LGPS) (single 46LiI-54Li$_3$PS$_4$ (LiI-LPS) vs a mixture of LiI-LPS and LGPS), were investigated. Operando DEP analysis revealed that the Gr electrodes using the LiI-LPS/LGPS mixtures showed much lower SOC (lower x in Li$_x$C$_6$) after charge, as compared to the case using the single LiI-LPS, which was due to a more severe side reaction for LGPS than for LiI-LPS.

2. Results and Discussion

2.1. NCM/Gr Cells with Varying n/p Ratios

Our first test vehicle for investigation by operando DEP analysis was a NCM/Gr all-solid-state three-electrode full cells with varied n/p ratios. Mechano-chemically prepared XRD-amorphous LiI-LPS showing Li$^+$ conductivity of 1.3 mS cm^{-1} at 30 °C was used as the SEs for the Gr electrodes while argyrodite Li$_6$PS$_5$Cl$_{0.5}$Br$_{0.5}$ showing Li$^+$ conductivity of 4.6 mS cm^{-1} at 30 °C was used for the NCM electrodes and SE layers (Figure S1, Supporting Information). NCM/Gr all-solid-state full cells with n/p ratios of 1.2, 1.4, and 1.7 were designed based on the results of first-cycle charge–discharge voltage profiles for NCM/Li-In and Gr/Li-In half cells at 30 °C, as illustrated in **Figure 1**a. The first charge–discharge voltage profiles for NCM/Gr full cells at 30 °C and their corresponding differential capacity (dQ/dV) plots are displayed in Figure 1b,c, respectively. The upper cutoff voltages
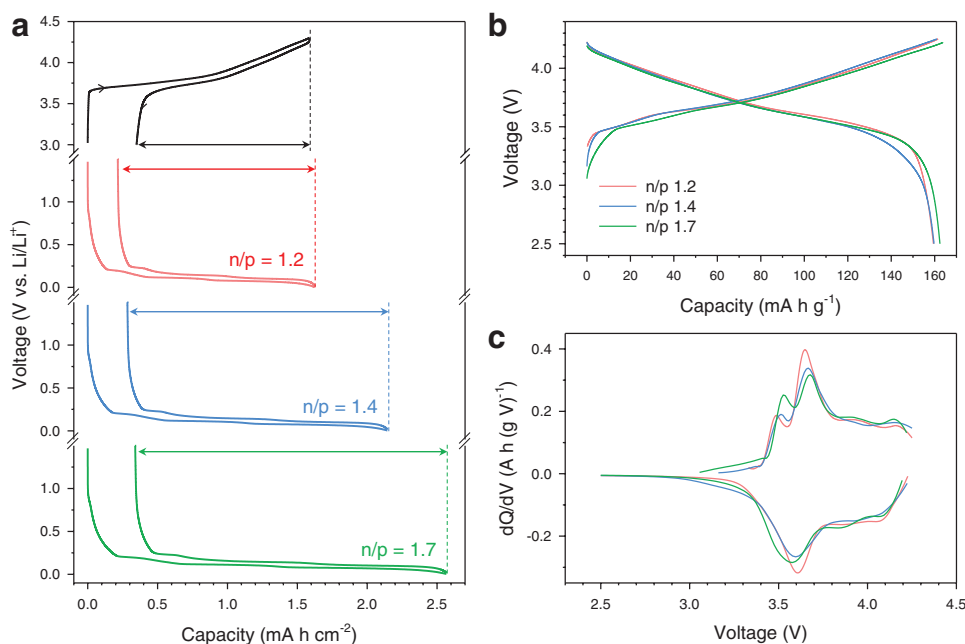

Figure 1. Results of NCM/Gr all-solid-state full cells with varied n/p ratios at 0.1C and 30 °C. a) First cycle charge–discharge voltage profiles of NCM/Li-In and Gr/Li-In half cells with different areal capacities of the Gr electrodes, indicating correspondingly varied n/p ratios. b) Second-cycle charge–discharge voltage profiles for NCM/Gr full cells with different n/p ratios at 0.1C and 30 °C and c) their corresponding differential capacity curves.

were regulated as 4.25, 4.25, and 4.22 V for the cells with n/p ratios of 1.2, 1.4, and 1.7, respectively, so that first charge capacities (or SOCs for NCM after charge) were held similar to each other. It was shown that first discharge capacities of NCM/Gr full cells were also almost identical, which was reasonable as discharge is ended by termination of the positive electrode, not the negative electrode, for all full cells, as estimated from the half cell results in Figure 1a and Figure S2 (Supporting Information). Importantly, assessments of voltage and differential capacity data alone are not enough for estimation of cell balancing or SOCs of full cells.

NCM/Gr three-electrode full cells, where Li-In as the reference electrode is in contact with a SE layer on top of the NCM electrode, were constructed,[46] and the pressure sensor was placed on top of the cells, as illustrated in **Figure 2**. This set-up allowed us to monitor the voltages of each electrode versus Li/Li+ and the corresponding overall pressure changes in real time. The transient voltages, pressure changes (ΔP), and differential pressure (dP/dt) during charge–discharge cycles could thus be obtained. The overall pressure changes in NCM/Gr cells followed those of Gr: the increasing pressure upon charge according to the lattice expansion of Gr (Figure S3, Supporting Information). This was due to the larger volumetric strain for Gr (Δvolume = +13%, $6C + Li^+ + e^- \rightarrow LiC_6$) than for NCM (e.g., Δvolume >≈4%, $Li[Ni,Mn,Co]O_2 \rightarrow Li_{1-x}[Ni,Mn,Co]O_2 + xLi^+ + xe^-$).[48,49] Cross-sectional SEM images of the Gr electrodes from NCM/Gr full cells with a n/p ratio of 1.2 during the first cycle are shown in Figure S4 in the Supporting Information. The pores existing among the particles and SEs before cycling are reduced upon charge, which clearly reflects the effects of volume expansion of Gr. Furthermore, we also constructed NCM/Li$_4$Ti$_5$O$_{12}$ (LTO) three-electrode full cells. Because the volumetric strain for LTO is marginal (0.2–0.3%, $Li_4Ti_5O_{12} + 3Li^+ + 3e^- \rightarrow Li_7Ti_5O_{12}$),[50] the overall pressure change signals for NCM/LTO cells could be regarded as information obtained solely from the NCM electrodes (Figure S5, Supporting Information). The decreasing pressure upon discharge (de-intercalation) agreed perfectly with the corresponding shrinkage of the NCM lattice due to the strengthened Coulombic repulsive forces between transition metal slabs.[17] By subtracting the pressure change signals of NCM/LTO cells from those of NCM/Gr cells, the Gr signals could be extracted, as shown in Figure S3 in the Supporting Information. Voltages of each electrode at the end of charge and discharge for NCM/Gr and NCM/LTO three-electrode full cells are summarized in Table S1 in the Supporting Information.

The resulting deconvoluted pressure change and time-derivative differential pressure (or DEP) curves for the Gr electrodes (ΔP_{Gr} and dP_{Gr}/dt) in NCM/Gr all-solid-state three-electrode full cells with varied n/p ratios are shown in **Figure 3**. The results during the initial three cycles are also provided in Figure S6 in the Supporting Information. Again, the gradually increasing pressure of the Gr electrodes in three-electrode full cells during charge (Li+ intercalation) was due to the corresponding volume expansion.[48] Importantly, the DEP profiles of the Gr electrodes featured the points of minimum and maximum values during charge and discharge, respectively (denoted as red diamonds). It is shown that the minimum DEP values during charging are shifted in the positive direction as the n/p ratio increases. For discharge, the maximum points
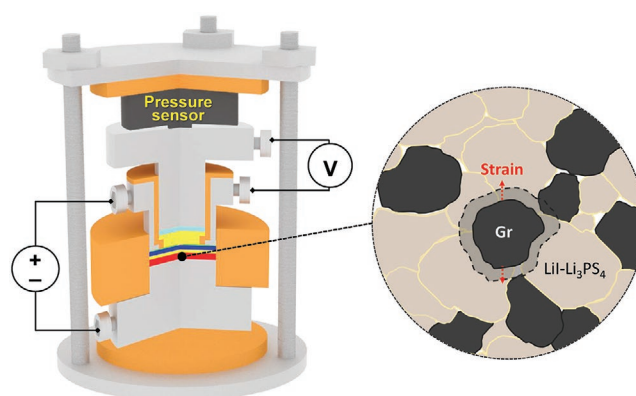

Figure 2. Schematic illustrating all-solid-state three-electrode cells combined with a pressure monitoring system. The pressure changes monitored are reflected by the volume changes of electrode active materials in the composite electrodes.

are shifted in the negative direction. This observation provides an important insight that the DEP profiles could be utilized as references for specific SOCs. During volume expansion of Gr upon Li+ intercalation, multiple phase transitions proceed, and their fractions and unit cell volumes determine the overall volume changes upon Li+ intercalation (or de-intercalation).[48] The volume changes in Gr as a function of SOC and their differential ($-dV/dSOC$) curves obtained from in situ XRD data in a previous work are shown in Figure S7 in the Supporting Information.[6,48] Notably, the $-dV/dSOC$ curve leaves characteristic signatures of specific SOCs, which could reflect the DEP profiles in Figure 3. Indeed, the overall shapes for the differential volume change and the DEP curves resemble each other. Moreover, their clear, common, maximum points could provide new references. A more detailed discussion follows later.

The next step was to verify our DEP-based protocol for SOC estimation. First, NCM/Gr full cells after charge and discharge were investigated using ex situ XRD measurements (**Figure 4**a). The acquisition of undisturbed ex situ XRD signals for Li$_x$C$_6$ was possible owing to the use of XRD-amorphous featured LiI-LPS used for the Gr electrodes (Figure S1, Supporting Information). After charging, NCM/Gr full cells with smaller n/p ratios clearly showed stronger peaks at ≈23.9°, corresponding to a highly lithiated phase (LiC$_6$),[48,51] and more gold-colored feature for the collected Gr electrodes (Figure 4a; Figure S8, Supporting Information), which is also an indicator of a higher degree of lithiation.[52,53] Moreover, the SOCs of Gr electrodes in NCM/Gr full cells at the end of charge were obtained by ex situ XRD analysis. A detailed procedure is described in the Experimental section. The SOC values (x in Li$_x$C$_6$) obtained at the end of charge were 0.94, 0.83, 0.54 for the cells with n/p ratios of 1.2, 1.4, and 1.7, respectively (Table S2, Supporting Information). Secondly, the SOC values at the end of discharge were obtained by comparative analysis using the Gr/Li-In half cell data. The detailed procedure is illustrated in Figure S9 in the Supporting Information. The difference in the resulting SOC values after discharge were marginal: $x = 0.05$, 0.04, and 0.02 for the cells with the n/p ratios of 1.2, 1.4, and 1.7, respectively (Table S3, Supporting Information), which was also consistent with the estimation by the consideration of NCM/Li-In and Gr/Li-In half cell data (Figure 1a).
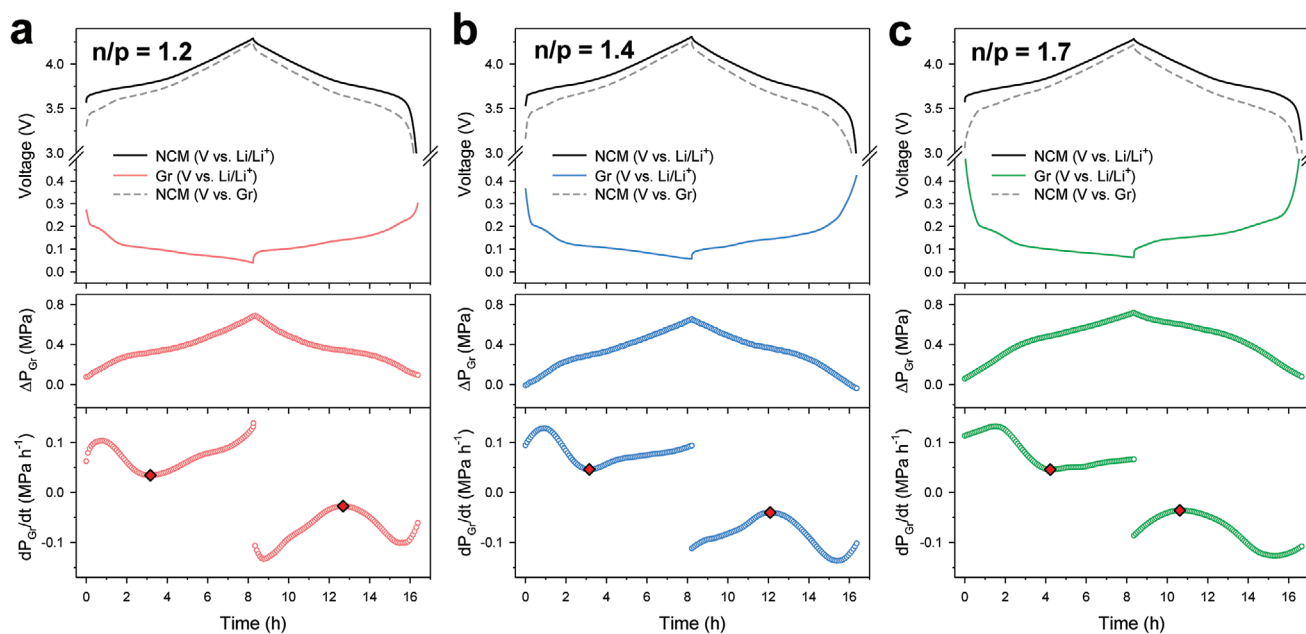
**ADVANCED
SCIENCE NEWS**
www.advancedsciencenews.com

**ADVANCED
FUNCTIONAL
MATERIALS**
www.afm-journal.de

Figure 3. Differential electrochemical pressiometry (DEP) results of NCM/Gr all-solid-state three-electrode cells with three different n/p ratios at 2nd cycle, 0.1C, and 30 °C. Charge discharge voltage profiles of each electrode, corresponding pressure change curves (ΔP), and DEP profiles (dP/dt) of Gr electrodes for NCM/Gr cells with n/p ratios of a) 1.2, b) 1.4, and c) 1.7. The minimum and maximum points for the DEP profiles during charge and discharge are indicated by the red diamonds.

Based on the as-obtained SOC values at the end of charge and discharge, the x-axes for second discharge voltages of the Gr electrodes in NCM/Gr full cells and corresponding DEP data were calibrated in terms of SOCs (x in Li_xC_6) and are displayed in Figure 4b–d. First, the SOCs at the maximum DEP points appear to be almost identical for all three cells: 0.45, 0.44, and 0.43 for the n/p ratios of 1.2, 1.4, and 1.7, respectively. Surprisingly, these values were also very close to that at the maximum differential volume change value ($-dV/dSOC$) of 0.46 in Figure S7 in the Supporting Information. Furthermore, the SOCs at the minimum DEP points were very similar among all three cells: 0.13, 0.13, and 0.11 for the n/p ratios of 1.2, 1.4, and 1.7, respectively (Figure 4b–d). In summary, the results thus far verify that the DEP-based SOC estimation protocol developed for ASBs is reliable.

Furthermore, voltage-derivative differential pressure (dP/dV) curves during discharge for the Gr electrodes in NCM/Gr full cells are compared with differential capacity (dQ/dV) curves in Figure S10 in the Supporting Information. The peak positions for dP/dV coincide with those for dQ/dV, indicating that pressure changes were responded upon voltage changes without dilation at the tested current (0.1C, 150 μA cm^{-2}).

2.2. NCM/Gr Cells with Different SEs in the Gr Electrodes: LiI-LPS versus (LiI-LPS + LGPS)

The encouraging result of the DEP-based SOC estimation protocol led us to investigate their application to a more complicated system, i.e., NCM/Gr all-solid-state full cells, for which reductively unstable LGPS were included in the Gr electrodes.[22,54,55] Two NCM/Gr full cells with the Gr electrodes employing LiI-LPS or a mixture of LiI-LPS and LGPS

(80:20 weight ratio, hereafter referred to as "(LiI-LPS + LGPS)") were thus selected as a model system. By simple thermodynamic consideration, full reduction products for LiI-LPS are LiI, Li_2S, and Li_3P.[55] As all the decomposition products are e$^-$ insulators, the Gr/LiI-LPS interfaces could be passivated well (**Figure 5a**). In stark contrast, full reduction of LGPS results in the formation of a detrimental mixed conductor of Li_xGe alloys (Figure 5b), which would cause severe reductive decomposition of electrolytes, thereby resulting in largely lowered initial CEs and increased interfacial resistances.[54]

Voltage profiles, corresponding pressure change, and DEP profiles for the Gr electrodes in NCM/Gr three-electrode full cells employing LiI-LPS and (LiI-LPS + LGPS) during first charge and discharge are displayed in Figure 5c,d, respectively. By including LGPS in the Gr electrodes, the initial CE was decreased from 79.7 to 54.1%. In the discharge voltage profiles of each electrode obtained using three-electrode cells, it was clearly shown that discharge is ended by termination of the Gr electrodes for the case including LGPS far earlier, as compared to the case excluding LGPS. This result reflects a much lower SOC of Gr after the initial charge for the case using (LiI-LPS + LGPS) than for the case using LiI-LPS, which was caused by the severe irreversible lithiation reaction in LGPS, originating from the poor passivating Gr-LGPS interfaces illustrated in Figure 5b.[54]

Despite the much lower SOC estimated after the initial charge for the case using (LiI-LPS + LGPS) than for the case using LiI-LPS, the corresponding pressure changes showed similar values: ΔP = +0.70 and +0.78 MPa, respectively. This result means that the contribution of the side reaction, i.e., LGPS lithiation, on the overall volume change of the Gr electrodes, should be as significant as that of Li$^+$ intercalation in Gr. The largely different shapes of the charge DEP profiles

**ADVANCED
SCIENCE NEWS**

www.advancedsciencenews.com

**ADVANCED
FUNCTIONAL
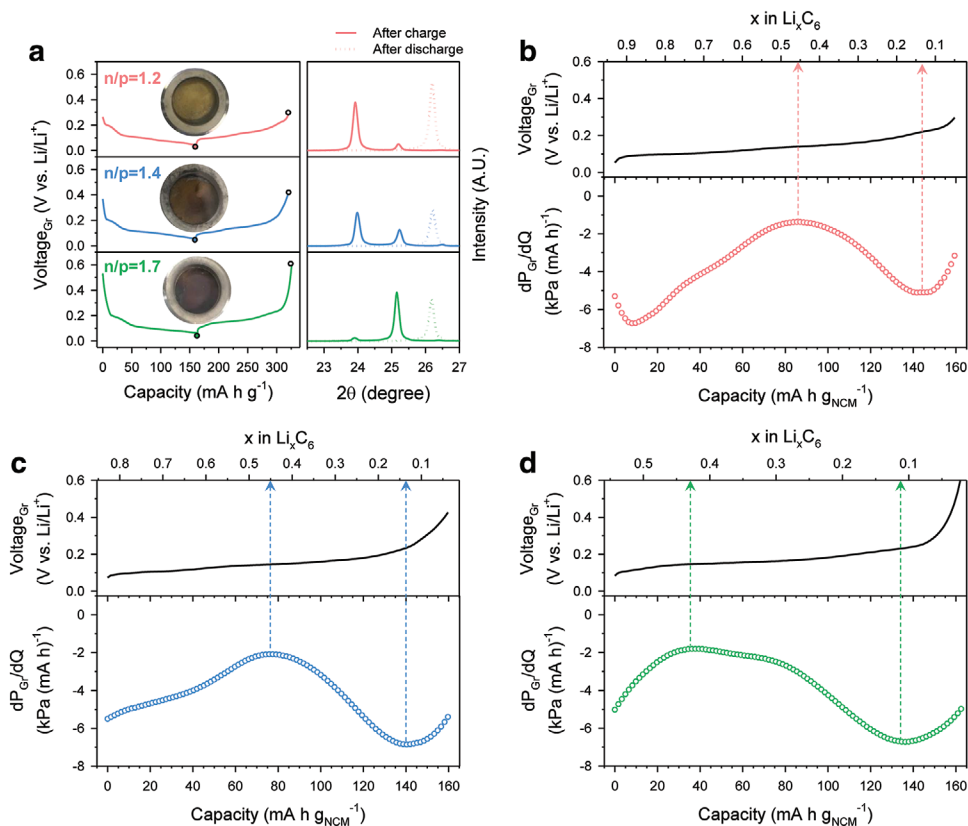MATERIALS**

www.afm-journal.de

Figure 4. Results of the state-of-charge (SOC) estimation by the DEP analysis for NCM/Gr all-solid-state full cells with three different n/p ratios at 30 °C. a) Ex situ XRD results for NCM/Gr cells wherein charge–discharge voltage profiles for the Gr electrodes at 0.1C and their corresponding ex situ XRD patterns after charge and discharge are shown. Photographs of the Gr electrodes from NCM/Gr full cells after charge are also displayed. b) Second discharge voltage profiles and their corresponding DEP profiles (dP/dQ) for the Gr electrodes of NCM/Gr cells with n/p ratios of b) 1.2, c) 1.4, and d) 1.7. Dashed vertical arrows indicate estimated SOCs. The SOCs of starting points of discharge were obtained by ex situ XRD analysis (Table S2, Supporting Information). The SOCs at the end of discharge were obtained by the analysis comparing with the results for NCM/Li-In half-cells (Figure S9 and Table S3, Supporting Information).

between the cases for LiI-LPS and (LiI-LPS + LGPS) are thus understood. In contrast, the main feature for the discharge DEP profile of the Gr electrodes, i.e., the appearance of a clear maximum point at which the SOC is estimated to be $x = 0.46$ in Li_xC_6, is preserved for the case using (LiI-LPS + LGPS). By ex situ XRD analysis (Figure S11, Supporting Information) and comparative analysis using the Gr/Li-In half cell data (Figure S12, Supporting Information), following the procedure described in Section 2.1, SOCs for Gr in NCM/Gr cells employing (LiI-LPS + LGPS) were obtained at the end of first charge and discharge, respectively: $x = 0.77$ and 0.02 in Li_xC_6 (Table S4, Supporting Information). The accordingly calibrated SOCs indicated the SOC value of $x = 0.49$ at the maximum DEP point (Figure S13, Supporting Information), which agrees well with the results for the cells using LiI-LPS (Figure 4) and thus verifies the generalized validity of DEP-based SOC estimation for discharge. Importantly, the large shift in the maximum discharge DEP point in the negative direction of discharge capacity for the case using (LiI-LPS + LGPS), as compared with the case using LiI-LPS, is well in line with the much lower SOCs of Gr after charge when combined with SEs containing LGPS, which was confirmed by three-electrode cell analysis.

3. Conclusion

In summary, a new operando DEP for all-solid-state batteries was successfully developed. Through the precise measurements of pressure changes of all-solid-state cells in real time, it was shown that the time- (or capacity-) derivative differential pressure, reflecting the corresponding volume changes of electrode active materials, could be correlated with the specific SOCs of all-solid-state cells. The SOC estimation of the Gr electrodes in NCM/Gr full cells with varied n/p ratios by the operando DEP analysis was demonstrated successfully; this was confirmed by the complementary analysis using a three-electrode cell and ex situ XRD measurements. Finally, the significantly delayed charging of the Gr electrode in NCM/Gr full cells at the initial cycle was disclosed by the operando DEP analysis for the case using reductively unstable LGPS, as compared with the case being free from LGPS. While our proof-of-concept was demonstrated for the Gr electrodes, it could also be applied to other electrode systems in all-solid-state cells, such as Li[Ni,Co,Mn]O₂ and Li metal. Li[Ni,Co,Mn]O₂ is known to suffer from severe electrochemo-mechanical degradation owing to the deleterious H2-H3 phase transition at >≈4.1 V (vs Li/Li⁺), which accompanies highly anisotropic and

**ADVANCED
SCIENCE NEWS**

www.advancedsciencenews.com

**ADVANCED
FUNCTIONAL
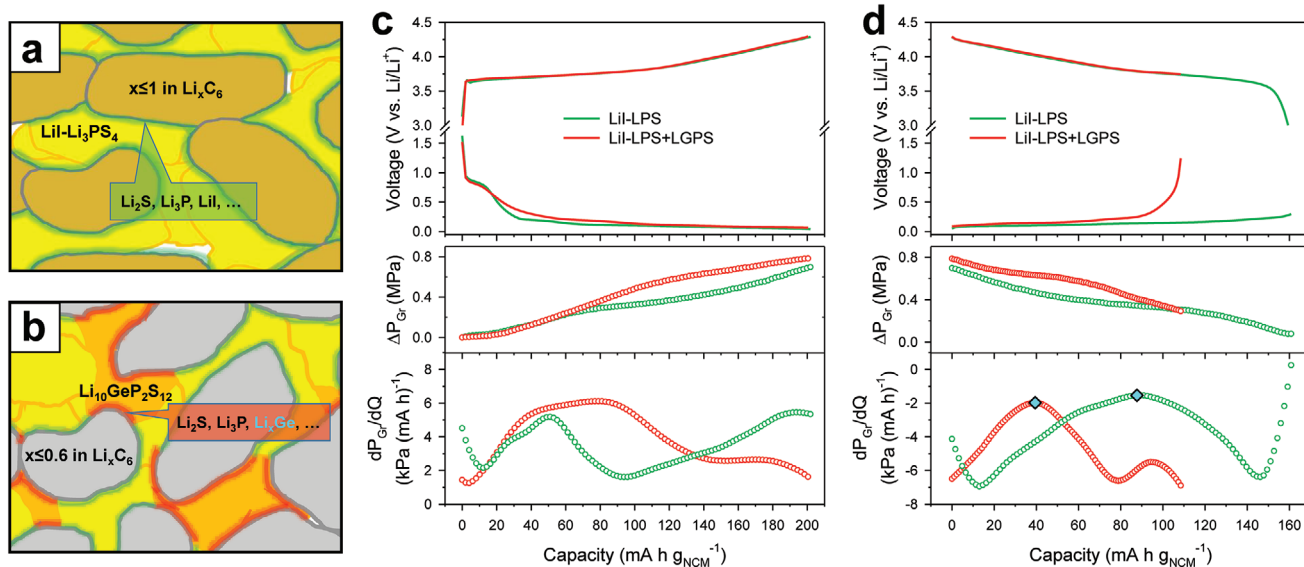MATERIALS**

www.afm-journal.de

Figure 5. Results of NCM/Gr all-solid-state three-electrode full cells at 0.1C and 30 °C, employing SEs without or with LGPS in their Gr electrodes. Schematic illustrating Gr electrodes employing a) LiI-LPS and b) (LiI-LPS + LGPS), after first charge. Note the more severe side reaction for the case when using LGPS due to the formation of detrimental mixed conductor Li_xGe, compared with the case when using LiI-LPS. First-cycle voltage profiles of the NCM and Gr electrodes, corresponding pressure changes, and DEP profiles for the Gr electrodes employing LiI-LPS versus (LiI-LPS + LGPS) (80:20 weight ratio) during c) charge and d) discharge at the initial cycle. The maximum discharge DEP points, where the SOC is estimated at $x = 0.46$ in Li_xC_6, are indicated as diamonds in the panel of (d). The n/p ratio for NCM/Gr cells was 1.2.

large volume changes.[16,56] The DEP profile at high voltages for NCM/Gr full cells in our result in Figure S3 in the Supporting Information (indicated by the arrows) may be used as the indicator for such an effect. Additionally, the degradation modes of Li metal, such as the penetrating growth through SE layers and interfacial reaction with the SEs,[22,41] could be diagnosed using the operando DEP analysis, which will be our future project. Practically important sheet-type electrodes employing soft polymeric binders could also be an interesting platform for investigation by the operando DEP measurement. Highly elastic polymeric binders in composite electrodes would show dynamic evolution in the response of local stresses generated by the volumetric strains of electrode active materials, such as pore-filling and squeezing penetration into interfaces, which is imperative for electrochemical performance and may be traced by the operando DEP measurement.[17,29,40,59] Moreover, the nondestructive feature of the developed operando DEP analysis protocol could provide an important benefit in the development of practical all-solid-state technology in terms of battery management systems.[57,58]

4. Experimental Section

Preparation of Materials: Argyrodite $Li_6PS_5Cl_{0.5}Br_{0.5}$ powders were prepared by mechanical-milling and subsequent heat-treatment under an Ar atmosphere. A stoichiometric mixture of Li_2S (99.9%, Alfa Aesar), P_2S_5 (99%, Sigma Aldrich), LiCl (99.99%, Sigma Aldrich), and LiBr (99.998%, Alfa Aesar) was ball-milled at 600 rpm for 10 h at room temperature in a ZrO_2 vial with ZrO_2 balls using a planetary ball mill (Pulverisette 7PL; Fritsch GmbH). The resulting powders were heat-treated at 550 °C for 5 h in a sealed fused silica tube. The as-prepared SE powders showed a Li-ion conductivity of 4.6 mS cm^{-1} at 30 °C. LiI-LPS

powders were prepared by mechanical-milling under an Ar atmosphere. A stoichiometric mixture of Li_2S, P_2S_5, and LiI (99.995%, Alfa Aesar) was ball-milled at 510 rpm for 10 h at room temperature in a ZrO_2 vial with ZrO_2 balls using a planetary ball mill. The as-prepared LiI-LPS was XRD-amorphous and showed a Li-ion conductivity of 1.3 mS cm^{-1} at 30 °C. For the preparation of $Li_{10}GeP_2S_{12}$ powders, a stoichiometric mixtures of Li_2S, P_2S_5, and GeS_2 (99.9%, American Elements) powders were pelletized under 370 MPa and put in a sealed quartz tube, followed by heat-treatment at 550 °C for 10 h. NCM particles coated with $LiNbO_3$ (1.4 wt%) via a wet-chemical method using lithium ethoxide (95%, Sigma Aldrich) and niobium ethoxide (99.95%, Sigma Aldrich) were used.[29]

Materials Characterization: For the ex situ XRD measurements, the samples were hermetically sealed by a Be window, mounted on a Rigaku MiniFlex 600 diffractometer, and measured with Cu K_α radiation between 10° and 70° of 2θ with a step size of 0.02° at 40 kV and 15 mA. For the SOC estimation of Gr in NCM/Gr full cells, the ex situ XRD data were refined by the Rietveld refinement method using the software Fullprof. The refinement was started with atomic coordinates reported by the reference.[51] The XRD peaks were modeled from pseudo-Voigt function and the background level was determined manually before being refined. The following parameters were initially refined: 1) scale factor, 2) lattice parameters, 3) variables for profile function, such as *U*, *V*, *W*, and shape, and 4) phase fractions. Cross-sectional FESEM images of Gr electrodes were obtained by polishing at 6 kV for 6 h or 4 kV for 3 h with an Ar ion beam (JEOL, IB19510CP). FESEM images and corresponding EDXS elemental maps were obtained using AURIGA (Carl Zeiss).

Electrochemical Characterization: The positive electrodes comprised of NCM, $Li_6PS_5Cl_{0.5}Br_{0.5}$, and conducting carbon additives (super C65) in a weight ratio of 70:30:3 were prepared by dry-mixing using mortar and pestle. The mass loading was 11.3 mg cm^{-2}. The Gr electrodes were obtained by mixing of natural graphites and LiI-LPS or (LiI-LPS + LGPS, weight ratio of 80:20) with the weight ratio of 60:40. The LTO electrodes were prepared by mixing LTO, $Li_6PS_5Cl_{0.5}Br_{0.5}$, conducting carbon additives (super C65), and solvate ionic liquid (Li(G3)TFSI, LiTFSI : lithium bis(trifluoromethanesulfonyl)imide), G3: triethylene glycol dimethyl ether) with a weight ratio of 10:9:1:0.1.[29] The reference electrodes, which were partially lithiated indium

(nominal composition of $Li_{0.5}In$), were prepared by mixing Li metal (FMC Lithium corp.) and In (Sigma-Aldrich, 99.99%) powders with or without SE powder. The all-solid-state three-electrode cells with a diameter of 13 mm, comprised of Ti rods as the current collectors and polyaryletheretherketone (PEEK) mold, were assembled by the following procedure, as described in the previous report:[46] First, SE layers were formed by pelletizing 150 mg of $Li_6PS_5Cl_{0.5}Br_{0.5}$ powders. Then, the as-prepared cathode mixtures were spread on one side of the SE layer while the counter electrode (Gr or LTO) was put on the other side; the whole assemblies were then pressed at 370 MPa. $Li_6PS_5Cl_{0.5}Br_{0.5}$ (60 mg) was put on top of the working electrode (Figure 2a). Finally, the $Li_{0.5}In$ powder, as the reference electrode, was put on the top of the as-put $Li_6PS_5Cl_{0.5}Br_{0.5}$ layer, followed by pressing at 74 MPa. The three-electrode full cells were cycled at 0.1C and 30 °C between 2.50–4.25 V, 2.50–4.25 V, and 2.50–4.22 V for the n/p ratios of 1.2, 1.4, and 1.7, respectively, in order to make the delithiated state of NCM identical. The galvanostatic charge–discharge cycling tests were carried out by applying the current between the working electrode and counter electrode while the open-circuit voltage of the working electrode/RE was measured. The applied pressure for all the fabricated cells before cycling was set to ≈74 MPa. For operando DEP measurements, pressure sensors with a resolution of 0.1 kg (load cell, BONGSHIN) were assembled with the three-electrode cells (Figure 2a). The pressure changes during charge and discharge were monitored using software created in-house.

Supporting Information

Acknowledgements

Conflict of Interest

The authors declare no conflict of interest.

Keywords

[1] N. S. Choi, Z. H. Chen, S. A. Freunberger, X. L. Ji, Y. K. Sun, K. Amine, G. Yushin, L. F. Nazar, J. Cho, P. G. Bruce, *Angew. Chem., Int. Ed.* **2012**, *51*, 9994.

[2] M. Ebner, F. Marone, M. Stampanoni, V. Wood, *Science* **2013**, *342*, 716.

[3] M. T. McDowell, S. W. Lee, W. D. Nix, Y. Cui, *Adv. Mater.* **2013**, *25*, 4966.

[4] J. W. Choi, D. Aurbach, *Nat. Rev. Mater.* **2016**, *1*, 16013.

[5] R. Schmuch, R. Wagner, G. Hörpel, T. Placke, M. Winter, *Nat. Energy* **2018**, *3*, 267.

[6] R. Koerver, W. Zhang, L. d. Biasi, S. Schweidler, A. O. Kondrakov, S. Kolling, T. Brezesinski, P. Hartmann, W. G. Zeier, J. Janek, *Energy Environ. Sci.* **2018**, *11*, 2142.

[7] Y. S. Jung, K. T. Lee, S. M. Oh, *Electrochim. Acta* **2007**, *52*, 7061.

[8] M.-H. Park, M. G. Kim, J. Joo, K. Kim, J. Kim, S. Ahn, Y. Cui, J. Cho, *Nano Lett.* **2009**, *9*, 3844.

[9] K. Feng, M. Li, W. W. Liu, A. G. Kashkooli, X. C. Xiao, M. Cai, Z. W. Chen, *Small* **2018**, *14*, 1702737.

[10] X. H. Zhang, D. B. Kong, X. L. Li, L. J. Zhi, *Adv. Funct. Mater.* **2019**, *29*, 1806061.

[11] S. Choi, T.-w. Kwon, A. Coskun, J. W. Choi, *Science* **2017**, *357*, 279.

[12] D. Mazouzi, B. Lestriez, L. Roué, D. Guyomard, *Electrochem. Solid-State Lett.* **2009**, *12*, A215.

[13] Z. Chen, L. Christensen, J. R. Dahn, *Electrochem. Commun.* **2003**, *5*, 919.

[14] N.-S. Choi, K. H. Yew, K. Y. Lee, M. Sung, H. Kim, S.-S. Kim, *J. Power Sources* **2006**, *161*, 1254.

[15] M. Nie, D. P. Abraham, Y. Chen, A. Bose, B. L. Lucht, *J. Phys. Chem. C* **2013**, *117*, 13403.

[16] M. Bianchini, M. Roca-Ayats, P. Hartmann, T. Brezesinski, J. Janek, *Angew. Chem., Int. Ed.* **2019**, *58*, 10434.

[17] S. H. Jung, U. H. Kim, J. H. Kim, S. Jun, C. S. Yoon, Y. S. Jung, Y. K. Sun, *Adv. Energy Mater.* **2020**, *10*, 1903360.

[18] W. Li, E. M. Erickson, A. Manthiram, *Nat. Energy* **2020**, *5*, 26.

[19] Y. Koyama, T. E. Chin, U. Rhyner, R. K. Holman, S. R. Hall, Y. M. Chiang, *Adv. Funct. Mater.* **2006**, *16*, 492.

[20] K. Liu, Y. Liu, D. Lin, A. Pei, Y. Cui, *Sci. Adv.* **2018**, *4*, eaas9820.

[21] Y. Kato, S. Hori, T. Saito, K. Suzuki, M. Hirayama, A. Mitsui, M. Yonemura, H. Iba, R. Kanno, *Nat. Energy* **2016**, *1*, 16030.

[22] K. H. Park, Q. Bai, D. H. Kim, D. Y. Oh, Y. Zhu, Y. Mo, Y. S. Jung, *Adv. Energy Mater.* **2018**, *8*, 1800035.

[23] Z. Zhang, Y. Shao, B. Lotsch, Y.-S. Hu, H. Li, J. Janek, L. F. Nazar, C. Nan, J. Maier, M. Armand, L. Chen, *Energy Environ. Sci.* **2018**, *11*, 1945.

[24] X. Li, J. liang, X. Yang, K. Adair, C. Wang, F. Zhao, X. Sun, *Energy Environ. Sci.* **2020**, https://doi.org/10.1039/C9EE03828K.

[25] R. Chen, Q. Li, X. Yu, L. Chen, H. Li, *Chem. Rev.* **2019**, https://doi.org/10.1021/acs.chemrev.9b00268.

[26] N. Kamaya, K. Homma, Y. Yamakawa, M. Hirayama, R. Kanno, M. Yonemura, T. Kamiyama, Y. Kato, S. Hama, K. Kawamoto, A. Mitsui, *Nat. Mater.* **2011**, *10*, 682.

[27] J. v. d. Broek, S. Afyon, J. L. M. Rupp, *Adv. Energy Mater.* **2016**, *6*, 1600736.

[28] X. Han, Y. Gong, K. K. Fu, X. He, G. T. Hitz, J. Dai, A. Pearse, B. Liu, H. Wang, G. Rubloff, Y. Mo, V. Thangadurai, E. D. Wachsman, L. Hu, *Nat. Mater.* **2017**, *16*, 572.

[29] D. Y. Oh, Y. J. Nam, K. H. Park, S. H. Jung, K. T. Kim, A. R. Ha, Y. S. Jung, *Adv. Energy Mater.* **2019**, *9*, 1802927.

[30] Y. Chen, Z. Wang, X. Li, X. Yao, C. Wang, Y. Li, W. Xue, D. Yu, S. Y. Kim, F. Yang, A. Kushima, G. Zhang, H. Huang, N. Wu, Y.-W. Mai, J. B. Goodenough, J. Li, *Nature* **2020**, *578*, 251.

[31] A. Sharafi, E. Kazyak, A. L. Davis, S. Yu, T. Thompson, D. J. Siegel, N. P. Dasgupta, J. Sakamoto, *Chem. Mater.* **2017**, *29*, 7961.

[32] Y. Xiao, Y. Wang, S.-H. Bo, J. C. Kim, L. J. Miara, G. Ceder, *Nat. Rev. Mater.* **2020**, *5*, 105.

[33] L. Zhou, A. Assoud, Q. Zhang, X. Wu, L. F. Nazar, *J. Am. Chem. Soc.* **2019**, *141*, 19002.

[34] X. He, Q. Bai, Y. Liu, A. M. Nolan, C. Ling, Y. Mo, *Adv. Energy Mater.* **2019**, *9*, 1902078.

[35] F. Han, A. S. Westover, J. Yue, X. Fan, F. Wang, M. Chi, D. N. Leonard, N. J. Dudney, H. Wang, C. Wang, *Nat. Energy* **2019**, *4*, 187.

ADVANCED
SCIENCE NEWS

www.advancedsciencenews.com

ADVANCED
FUNCTIONAL
MATERIALS

www.afm-journal.de

[36] D. H. Kim, Y.-H. Lee, Y. B. Song, H. Kwak, S.-Y. Lee, Y. S. Jung, *ACS Energy Lett.* **2020**, *5*, 718.

[37] R. Koerver, I. Aygün, T. Leichtweiß, C. Dietrich, W. Zhang, J. O. Binder, P. Hartmann, W. G. Zeier, J. Janek, *Chem. Mater.* **2017**, *29*, 5574.

[38] K. N. Wood, K. X. Steirer, S. E. Hafner, C. Ban, S. Santhanagopalan, S.-H. Lee, G. Teeter, *Nat. Commun.* **2018**, *9*, 2490.

[39] D. M. Piper, T. A. Yersak, S.-H. Lee, *J. Electrochem. Soc.* **2013**, *160*, A77.

[40] W. Zhang, D. Schroeder, T. Arlt, I. Manke, R. Koerver, R. Pinedo, D. A. Weber, J. Sann, W. G. Zeier, J. Janek, *J. Mater. Chem. A* **2017**, *5*, 9929.

[41] L. Porz, T. Swamy, B. W. Sheldon, D. Rettenwander, T. Frömling, H. L. Thaman, S. Berendts, R. Uecker, W. C. Carter, Y.-M. Chiang, *Adv. Energy Mater.* **2017**, *7*, 1701003.

[42] D. H. Kim, H. A. Lee, Y. B. Song, J. W. Park, S. M. Lee, Y. S. Jung, *J. Power Sources* **2019**, *426*, 143.

[43] Y.-G. Lee, S. Fujiki, C. Jung, N. Suzuki, N. Yashiro, R. Omoda, D.-S. Ko, T. Shiratsuchi, T. Sugimoto, S. Ryu, J. H. Ku, T. Watanabe, Y. Park, Y. Aihara, D. Im, I. T. Han, *Nat. Energy* **2020**, *5*, 299.

[44] T. Krauskopf, H. Hartmann, W. G. Zeier, J. Janek, *ACS Appl. Mater. Interfaces* **2019**, *11*, 14463.

[45] J. Kasemchainan, S. Zekoll, D. S. Jolly, Z. Ning, G. O. Hartley, J. Marrow, P. G. Bruce, *Nat. Mater.* **2019**, *18*, 1105.

[46] Y. J. Nam, K. H. Park, D. Y. Oh, W. H. An, Y. S. Jung, *J. Mater. Chem. A* **2018**, *6*, 14867.

[47] L. Duchêne, D. H. Kim, Y. B. Song, S. Jun, R. Moury, A. Remhof, H. Hagemann, Y. S. Jung, C. Battaglia, *Energy Storage Mater.* **2020**, *26*, 543.

[48] S. Schweidler, L. de Biasi, A. Schiele, P. Hartmann, T. Brezesinski, J. Janek, *J. Phys. Chem. C* **2018**, *122*, 8829.

[49] A. O. Kondrakov, A. Schmidt, J. Xu, H. Geßwein, R. Mönig, P. Hartmann, H. Sommer, T. Brezesinski, J. Janek, *J. Phys. Chem. C* **2017**, *121*, 3286.

[50] T. Ohzuku, A. Ueda, N. Yamamoto, *J. Electrochem. Soc.* **1995**, *142*, 1431.

[51] A. Missyul, I. Bolshakov, R. Shpanchenko, *Powder Diffr.* **2017**, *32*, S56.

[52] P. Maire, A. Evans, H. Kaiser, W. Scheifele, P. Novák, *J. Electrochem. Soc.* **2008**, *155*, A862.

[53] M. Otoyama, H. Kowada, A. Sakuda, M. Tatsumisago, A. Hayashi, *J. Phys. Chem. Lett.* **2020**, *11*, 900.

[54] B. R. Shin, Y. J. Nam, D. Y. Oh, D. H. Kim, J. W. Kim, Y. S. Jung, *Electrochim. Acta* **2014**, *146*, 395.

[55] Y. Zhu, X. He, Y. Mo, *ACS Appl. Mater. Interfaces* **2015**, *7*, 23685.

[56] R. Jung, M. Metzger, F. Maglia, C. Stinner, H. A. Gasteiger, *J. Electrochem. Soc.* **2017**, *164*, A1361.

[57] L. G. Lu, X. B. Han, J. Q. Li, J. F. Hua, M. G. Ouyang, *J. Power Sources* **2013**, *226*, 272.

[58] H. J. Kim, Y. Park, Y. Kwon, J. Shin, Y.-H. Kim, H.-S. Ahn, R. Yazamic, J. W. Choi, *Energy Environ. Sci.* **2020**, *13*, 286.

[59] A. Bielefeld, D. A. Weber, J. Janek, *ACS Appl. Mater. Interfaces* **2020**, *12*, 12821.